Journal of Catalysis **208,** 393–403 (2002)
doi:10.1006/jcat.2002.3576

H_2 Production from Ethanol over Rh–Pt/CeO_2 Catalysts: The Role of Rh for the Efficient Dissociation of the Carbon–Carbon Bond

P.-Y. Sheng, A. Yee, G. A. Bowmaker, and H. Idriss[1]

Department of Chemistry, The University of Auckland, Private Bag 92019, Auckland, New Zealand

Received November 7, 2001; revised February 7, 2002; accepted February 21, 2002

The reaction of ethanol over a Rh–Pt/CeO_2 catalyst has been investigated by temperature-programmed desorption (TPD) and infrared spectroscopy (FTIR) and in steady state conditions. On the unreduced surface, ethoxides (the main species observed upon ethanol adsorption) are directly dehydrogenated to adsorbed acetaldehyde (η^1 mode at 1705 cm^{-1}, IR) that desorbs at 390 and 450 K (TPD). Comparison with TPD of ethanol over Pt/CeO_2 and Rh/CeO_2 separately shows that acetaldehyde desorption at 390 K is characteristic of the former and that at 450 K is characteristic of the latter. In contrast to this, on an H_2-reduced Rh–Pt/CeO_2 surface, ethoxide is directly decomposed to adsorbed CO (2032 cm^{-1}, IR), most likely via an oxametallacycle intermediate on Rh, with the formation of only very small amounts of acetaldehyde. This results in a considerable shift of the primary reaction product from acetaldehyde to CO and methane (TPD). Steady state reactions show that large amounts of H_2 can be formed depending on the ethanol-to-O_2 ratio and reaction temperature. At an O_2 : ethanol ratio = 2 and a reaction temperature above 600 K, total conversion of ethanol with an H_2 yield approaching 25 mol% is seen. Dehydration to ethylene was not observed under any of the reaction conditions investigated. Moreover, large amounts of CO were converted to CO_2, as evidenced by high CO_2-to-CO ratios (between 7 and 10). It appears that both Rh and Pt are required for efficient low-temperature production of H_2 from ethanol.

I. INTRODUCTION

Among all the candidates for possible alternative fuels, hydrogen holds a preeminent position because of its high energy content and environmental compatibility. The greatest potential use for hydrogen as vehicle fuel is when used in a fuel cell. Moreover, the use of hydrogen as a fuel offers an important reduction in NO_x, CO, and CO_2 emissions. There are four basic methods for hydrogen production at present: water electrolysis, gasification reactions, partial oxidation reactions of heavy oil, and steam reforming reactions (1).

H_2 production from alcohols is of major interest for molten carbonate fuel cells (2). H_2 can be made efficiently from methanol (retrosynthesis since methanol is in fact made from CO and H_2) (3). Ethanol as a source of H_2 has several advantages compared to methanol. It can be manufactured by fermentation of crops and as such has an attractive potential because of its origin (agroproduct) and the consequent reduction in carbon dioxide emission (1).

Compared to methanol ethanol has one major complication if one considers its total decomposition: it contains a carbon–carbon bond and as such requires a surface capable of breaking the carbon–carbon bond. There are at least two further requirements for the surfce. It must be capable of selectively oxidizing both carbon atoms to CO_2 and, in the case of hydrogen production, it must not be active (or must be relatively inactive) for the oxidation of H_2 to H_2O.

The following equations probably best describe the ideal processes:

$$CH_3CH_2OH_{(g)} + 1/2O_2 \rightarrow 3H_2 + 2CO_{(g)} \quad \Delta G_f^\circ = -105.9 \text{kJ mol}^{-1}, \qquad [1]$$

$$CH_3CH_2OH_{(g)} + 3/2O_2 \rightarrow 3H_2 + 2CO_{2(g)} \quad \Delta G_f^\circ = -620.3 \text{ kJ mol}^{-1}, \qquad [2]$$

$$CH_3CH_2OH_{(g)} + 2O_2 \rightarrow 3H_2O_{(g)} + 2CO_{(g)} \quad \Delta G_f^\circ = -517.3 \text{ kJ mol}^{-1}, \qquad [3]$$

$$CH_3CH_2OH_{(g)} + 3O_2 \rightarrow 3H_2O_{(g)} + 2CO_{2(g)} \quad \Delta G_f^\circ = -1306.1 \text{ kJ mol}^{-1}. \qquad [4]$$

The objective is to obtain a catalyst capable of orienting for reaction 2.

The reactions of alcohols over the surfaces of oxides have been studied for several decades now. A more comprehensive review of the reactivity of primary alcohols over some oxides can be found in Ref. (4). Several reactions have been observed, mainly dehydrogenation to aldehydes (5) and dehydration to olefins (such as on γ-Al_2O_3 (3, 6)). However, the majority of reactions observed from alcohols are usually due to secondary reactions of these primary products (7–17). Consequently the choice of the support is very crucial. An ideal support would not favor dehydration reactions (otherwise polymer formation may occur) and would

[1] To whom correspondence should be addressed. E-mail: h.idriss@auckland.ac.nz.

0021-9517/02 $35.00

have no (or mild) capacity for other C–C bond formation reactions (e.g., making higher unsaturated aldehydes by aldolization reactions).

Similarly, the reaction pathways of ethanol over well-defined metal surfaces have been studied in some depth. A summary of the different pathways over the metal surfaces can be found in Ref. (18). It is worth mentioning, however, that Rh stands alone, in some respects, vis à vis the reaction of ethanol. Although it does form ethoxides on the surface (similarly to other metals, such as Pt (19), Pd (20), and Ni (21)), dehydrogenation of these ethoxide does not yield acetaldehyde; instead it yields a stable oxametallacycle intermediate, $_{(a)}OCH_2CH_{2\text{-}(a)}$, which decomposes to CO at high temperatures (10).

In addition to some catalytic studies, we have previously investigated the reactions of ethanol over CeO_2 (8), Pd/CeO_2 (8), Pt/CeO_2 (22), and Rh/CeO_2 (23) by temperature-programmed desorption (TPD) and Fourier transform infrared spectroscopy (FTIR). Over CeO_2, a small part of ethanol is converted to acetaldehyde. Some of the acetaldehyde is oxidized on the surface to stable acetate species (IR) that decompose to CO, CO_2, and CH_4 (TPD). The addition of Pd or Pt results in partial reduction of the support (XPS) (8, 22, 23), which in turn suppresses the formation of surface acetates (8, 22, 23), as well as a decrease in the amount of CO_2 produced during TPD (20). Considerable amounts of benzene were however formed when Pd or Pt was used. In contrast, the presence of Rh results in the suppression of benzene production (23). This was interpreted as being due to the efficient carbon–carbon bond dissociation activity of Rh when compared to the other two metals. It is well-known that Rh is a good metal for C–C bond formation in a reducing atmosphere (24). It is thus not surprising that Rh (or Rh^{x+}) is active for carbon–carbon bond dissociation in an oxidizing environment. However, because of cocking Rh is not sufficiently active for the total decomposition of ethanol, and a second metal is needed to enhance either the hydrogenation or the oxidation pathway. These latter points have motivated the present work, which is devoted to investigating the combined activity of Rh–Pt with respect to the catalytic reaction of ethanol (Rh–Pd catalyst has very similar effects (25)). We have observed that the resulting catalyst is indeed active for the transformation of ethanol into CO_2 and H_2, depending on the operational conditions. An attempt to understand the reason for this activity is given based on parallel studies by TPD and FTIR, in addition to catalytic reaction studies.

II. EXPERIMENTAL

II.A. FTIR

IR experiments were performed with a Digilab FTS-60 FT spectrometer at a resolution of 4 cm^{-1} and 100 scans per spectrum. Experimental details have been published previously (8). Ethanol, cleaned by freeze–thaw pump cycles, was introduced (1.5 Torr) onto the sample (cleaned by successive heating in O_2 at ca. 700 K) maintained at ca. 300 K. The dosed sample was sequentially heated, in 50-K increments, to 673 K, and spectra were collected after cooling to ca. 300 K each time. Spectra are shown after subtraction (spectrum after dosing with ethanol minus spectrum of the clean sample).

II.B. TPD

A detailed description of the apparatus and experimental procedure can be found in Ref. (8). Relative yields were calculated following the method described in Ref. (26). The method of peak identification and analysis can be found in Ref. (12). Initially all masses up to 100 amu were scanned at different sensitivity ranges. Following the identification of desorption fragments, several runs were conducted at higher resolution (12 masses were recorded each time at a cycling rate of ca. 2 s), each time with a fresh sample to ensure reproducibility. The sample weight was ca. 50 mg.

II.C. Steady State Reactions

Experiments were conduced in a fixed-bed flow reactor at a pressure of 1 atm. Several gas chromatographs were used to monitor the reaction products: FID for hydrocarbons, and several TCDs for O_2, CO, CO_2, and H_2. Calibration of detector response was conducted for each product to ensure the linearity needed for quantitative analysis. For calculation of the activation energy (Table 1), the reactor was maintained at a differential mode (conversion less than ca. 10%). Ethanol was kept in a saturator maintained at different temperatures (from 273 to 337 K) in order to change its partial pressure in the reaction gas. Data was collected under steady state conditions with flow rate, $F = 0.265$ L/min (STP), catalyst weight, $W = 5 \times 10^{-2}$ g, and ethanol concentration, $C_{\text{Ethanol}} \approx 3 \times 10^{-3}$ mol/L (STP).

II.D. Catalyst Preparation and Characterization

CeO_2 was prepared from cerium(III) nitrate as described previously (8). CeO_2 powder was impregnated with Rh (ex $RhCl_3$) and Pt (ex $PtCl_2$) in the appropriate ratio to give 1 wt% Rh and 1 wt% Pt/CeO_2. After calcination in air at 573 K, the catalyst possessed a BET surface area comparable to that of CeO_2 alone. XRD and XPS (see Refs. (22, 23) for more details) were also performed; the results are summarized in Table 1. The number of molecules of ethanol, converted per surface atoms and per second, at 400 K, were calculated as follows. The rate of ethanol reaction $= 4.43 \times 10^{-6}$ mol g^{-1} $s^{-1} = 1.23 \times 10^{-7}$ mol m^{-2} $s^{-1} = 7.38 \times 10^{16}$ molecules m^{-2} s^{-1}. Assuming that each square meter contains 10^{19} atoms and since the surface is composed of 0.42% Pt and Rh atoms (the remaining being

TABLE 1

Surface and Bulk Characterization of CeO_2 and M/CeO_2 Catalysts, Together with Kinetic Parameters for Ethanol Oxidation

Catalyst	CeO_2[8]	Pt/CeO_2[22]	Rh/CeO_2[23]	Rh–Pt/CeO_2[a]
Surface area ($m^2\ g^{-1}$)	57	63	49	36
XPS M ($3d_{5/2}$, $4f_{7/2}$) (eV)	—	74.0 (PtO)	309.5 (RhO_2)	310.0, 73.0
XPS O (1s)/ Ce (3d)	2.44	1.59	1.91	1.66
XPS at%	—	0.26	0.17	0.21, 0.21
E_a (kJ mol^{-1})[b]	75	43	49	34
TON[c] at 400 K	—	2.6	5.9	1.76

[a] This work.
[b] Computed in the 300- to 573-K range.
[c] TON, number of molecules of ethanol converted per surface metal atom per second.

Ce, O, and some C), then the rate of per metal atoms is

$$7.38E16\frac{\text{molecules}}{\text{m}^2\ \text{s}}\frac{1}{4.2E16}\frac{\text{m}^2}{\text{atoms}} = 1.76\frac{\text{molecules}}{\text{atoms}}.$$

The reactivity of CeO_2 alone is negligible at 400 K.

III. RESULTS

III.A. TPD

Figure 1 shows TPD after ethanol adsorption at 300 K over Rh–Pt/CeO_2. Several products were desorbed in multiple temperature domains. Despite the large number of products, the analysis is in fact relatively simple because of the desorption of products over distinct temperature domains. The observed major and minor products and the calculated carbon yield are shown in Table 2. The combined experimental and statistical (several runs) error is estimated to be in the range of 15–20%. The major products are those shown without multiplication factors in Fig. 1. There are four main carbon-containing products: ethanol (unreacted), acetaldehyde (primary reaction product), methane (primary or secondary reaction product), and CO/CO_2 (decomposition/total oxidation), water is also desorbing with some H_2 as the non-carbon-containing products. The above four carbon-containing products contribute ca. 97% of the total carbon yield. Other minor products (mainly due to secondary reaction of acetaldehyde) included butene, crotonaldehyde, ketene, and possibly propene. All these products constituted ca. 3% of the total carbon yield. Ethylene is not observed, which means that the dehydration pathway does not occur. Almost no benzene formation was seen, in contrast to the relatively significant benzene desorption observed on both Pd/CeO_2 (8) and Pt/CeO_2 (22) surfaces. The relatively high CO_2-to-CO ratio (ca. 8) is indicative of the ease of removing O from the surface. The reasons for

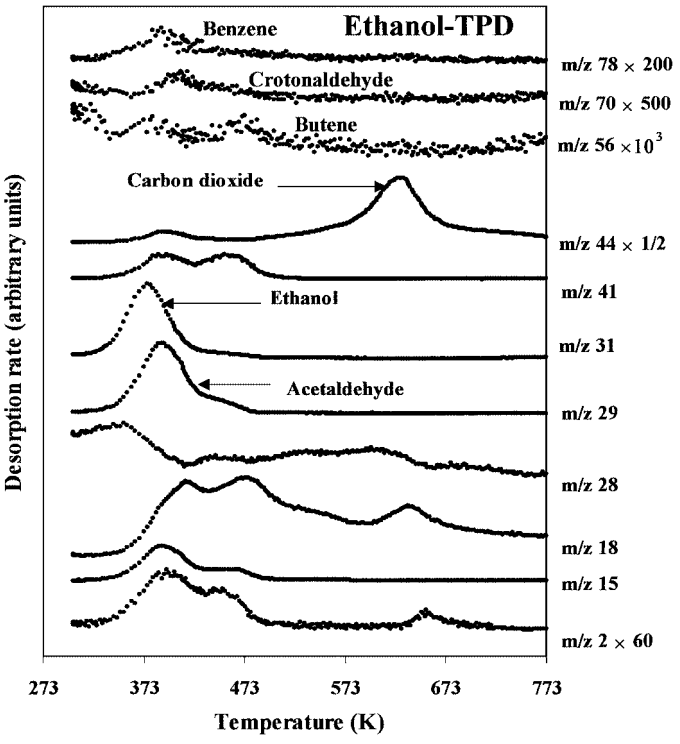

FIG. 1. TPD after ethanol adsorption at 300 K over unreduced Rh–Pt/CeO_2.

the nature and distribution of these products are discussed below.

TPD from H_2-reduced Rh–Pt/CeO_2 was also examined and the results are shown in Table 3. The major difference is the change in the main reaction product from acetaldehyde to methane; the ratio of acetaldehyde to methane decreased 20-fold, from 3.75 (unreduced) to ca. 0.18 (reduced). This is probably consistent with the role of Rh metal, where

TABLE 2

Product Distribution During Ethanol TPD over Unreduced Rh–Pt/CeO_2

Product	Desorption temperature (K)	% Carbon yield	% Carbon selectivity
Hydrogen (m/e, 2)	395, 445, 655	—	—
Water (m/e, 18)	415, 475, 635	—	—
Major products			
Methane	390, 450	6.52	9.69
Carbon monoxide	530, 605	6.51	9.67
Carbon dioxide	625	26.99	40.11
Acetaldehyde	390, 450	24.48	36.38
Ethanol	375, 450	32.71	—
Minor products			
Ketene (m/e, 42, 41)	455	2.31	3.43
Benzene (m/e, 78)	390	0.33	0.49
Butene (m/e, 56)	465	0.08	0.12
Crotonaldehyde (m/e, 70)	410	0.07	0.11

TABLE 3

Product Distribution during Ethanol TPD over H_2-Reduced Rh–Pt/CeO_2

Product	Desorption temperature (K)	% Carbon yield	% Carbon selectivity
Hydrogen	445, 655	—	—
Water	415, 475, 635	—	—
Methane	460, 670	13.2, 7.5	24.7, 14.0
Carbon monoxide	670	19.22	35.9
Carbon dioxide	670	9.7	18.1
Acetaldehyde	460	3.8	7.1
Ethanol	430	46.5	—
Other products[a]	400–500	—	—

[a] Benzene was not observed; butene and crotonaldehyde together contributed by less than 0.05%.

ethoxides are dehydrogenated not to acetaldehyde but to an oxametallacycle intermediate (13) (see discussion section below for more details). Peak temperature shifts also occurred for some products. Both CO and CO_2 desorbed at higher temperatures. In addition methane desorbed in a second peak at 670 K. It is clear that the metallic state, formed upon H_2 reduction, is responsible for these changes. The high-temperature desorption of methane, concomitant with both CO and H_2, is most likely formed by syngas conversion on Pt and Rh metals.

III.B. Infrared

FTIR of ethanol over CeO_2 (8), Pd/CeO_2 (8), Pt/CeO_2 (22), and Rh/CeO_2 (23) has been previously investigated. Several species were observed depending on the nature of the surface, its prior treatment, and the reaction temperature. The following main points from that work are as follows: (i) Ethoxides were observed on all surfaces upon dosing at room temperature. (ii) Acetates (formed via oxidation of ethoxides) were mainly detected on CeO_2; addition of any of the above metals resulted in almost complete elimination of the oxidation route at low temperatures. (iii) η^1-adsorbed acetaldehyde was mainly observed on the unreduced M/CeO_2 surfaces. (iv) CO was mainly observed on Rh/CeO_2 and the amount detected increased tremendously on the H_2-reduced Rh/CeO_2.

III.B.i. Adsorption of ethanol on Rh/CeO_2. The last point is shown in Fig. 2, where ethanol was adsorbed at 310 K over unreduced Rh/CeO_2 (Fig. 2a) and over H_2-reduced Rh/CeO_2 (Fig. 2b). In both cases bands related to ethoxides were seen as shown in Table 4. Other bands were also observed and included a peak at 1265 cm^{-1} (attributed to δOH), indicating the presence of molecularly adsorbed ethanol. The main difference between the two surfaces is the following: the presence of considerable amounts of adsorbed CO (2041 (linear) and 1904 (bridging) cm^{-1}) on the H_2-reduced Rh/CeO_2 with very little formation of adsorbed acetaldehyde. Conversely, considerable formation of acetaldehyde (νC–O of the η^1 mode at 1704 cm^{-1}) and very little formation of CO were seen on the unreduced Rh/CeO_2. There is also a negative peak at 1620 cm^{-1} attributed to δH_2O that has been displaced by ethanol.

Other details of the gas-phase reaction products as well as surface adsorbates as a function of temperature over the monometallic catalysts can be obtained from Refs. (8, 22, 23). The focus in this work is on the bimetallic Rh–Pt/CeO_2; parallel work has been conducted on Rh–Pd/CeO_2 (25). In general there is little difference between both bimetallic catalysts (with the exception of more acetaldehyde formation over Rh–Pd/CeO_2 compared to Rh–Pt/CeO_2).

III.B.ii. Adsorption of ethanol on unreduced Rh–Pt/CeO_2. The IR spectra of surface species formed upon ethanol adsorption on unreduced Rh–Pt/CeO_2 at 310 K are presented in Fig. 3. Ethanol was found not only to adsorb as ethoxide at 310 K but also to undergo dehydrogenation to form η^1-acetaldehyde. The spectrum in Fig. 3 (310 K) shows bands at 2934, 2907, 2880, 1478, 1453, 1397,

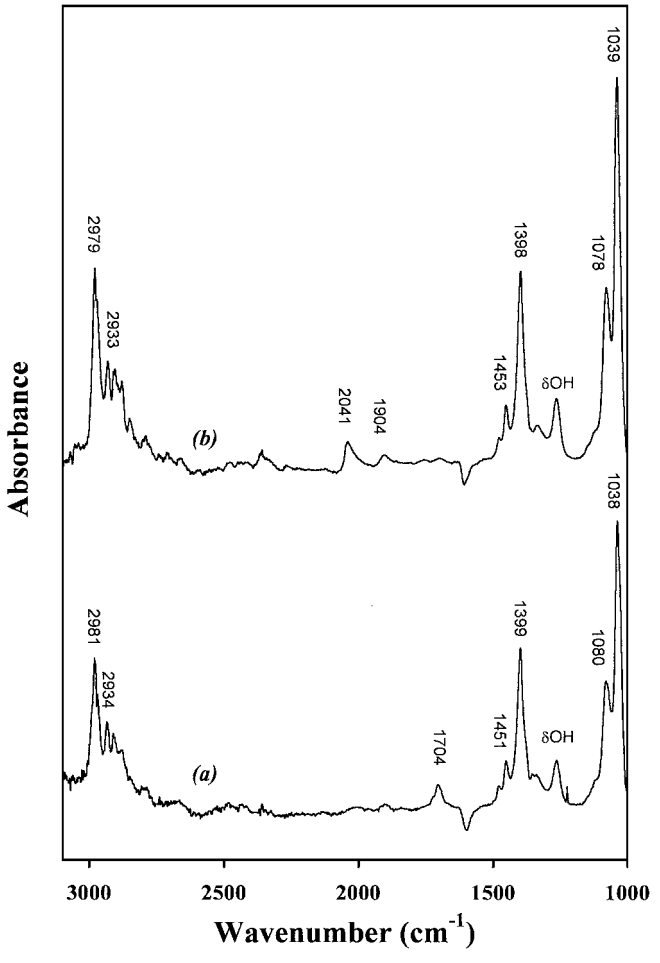

FIG. 2. FTIR after ethanol adsorption at 310 K over (a) unreduced Rh/CeO_2 and (b) H_2-reduced Rh/CeO_2.

TABLE 4

IR Vibrational Frequencies and Mode Assignments for Species Formed upon the Adsorption of Ethanol on Rh/CeO_2 at 310 K (Unless Indicated Otherwise) and Various Other Catalysts

Vibrational mode	CeO_2[5]	Al_2O_3[23]	TiO_2[24]	Pd/CeO_2[5]	Pt/CeO_2[19]	Rh/CeO_2[a]	Rh–Pt/CeO_2[a]
Ethanol–ethoxides							
$\nu_{as}(CH_3)$	2960	2970	2971	2982	2977	2981	2977
$\nu_{as}(CH_2)$	—	2930	2931	2934	2933	2934	2934
$\nu_s(CH_3)$	2836	2900	—	2909	2912	2911	2907
$\nu_s(CH_2)$	—	2870	2870	2880	2878	2878	2880
$\delta_{as}(CH_2)$	1473	—	1473	1478	1480	1478	1478
$\delta_{as}(CH_3)$	—	1450	1447	1451	1451	1450	1453
$\delta_s(CH_3)$	1383	1390	1379	1397	1399	1399	1397
$\delta_s(CH_2)$	—	—	—	—	—	1371	
$\omega(CH_2)$	—	—	1356	—	—	1350	
ν(CO) mono	1107	1115	1119	1078	1081	1080	1078
ν(CO)/ν(CC)	—	—	—	—	—	—	
ν(CO) bi	1057	1070	1042	1037	1037	1038	1030
CO							
νCO linear						2041	2032[b]
νCO bridging					1902 vw[c]	1904	1897 vw
Acetaldehyde							
νCO (η_1)				1705[d]	1704	1705	1705
H_2O–OH							
δOH					1264	1260	1264
δH_2O					1601	1600	1600

[a] This work.
[b] H_2 reduced.
[c] vw, Very weak.
[d] Weak and depends on reaction temperature and prior treatments.

1264, 1078, and 1038 cm^{-1}, which are attributed to the $\nu_{as}(CH_2)$, $\nu_s(CH_2)$, $\nu_s(CH_3)$, $\delta(CH_2)$, $\delta_{as}(CH_3)$, $\delta_s(CH_3)$, δ(OH), ν(C–O), and ν(C–O) modes of adsorbed ethoxides and ethanol, respectively, while the band at 1705 cm^{-1} corresponds to the ν(C=O) of adsorbed acetaldehyde. The maximum of the band situated at ca. 2977 cm^{-1} corresponding to the $\nu_{as}(CH_3)$ of the ethoxides is not clearly identified due to noise.

Upon heating the system to 373 K the band at 1705 cm^{-1} increased and two bands appeared, at 1660 and 1635 cm^{-1}, which are similar to those observed on unreduced Pd/CeO_2 (8). An increase in the temperature to 423 K resulted in a slight increase in the intensity of the 1660- and 1635-cm^{-1} bands but decreased the intensity of the 1705-cm^{-1} band. By 473 K the bands at 1705, 1660, and 1635 cm^{-1} had disappeared. The bands at 1660 and 1635 cm^{-1} are attributed to the ν(C=O) and ν(C=C) of adsorbed crotonaldehyde formed from the aldol condensation of acetaldehyde. The disappearance of these bands is very consistent with TPD results (compare Figs. 3 and 1). Bands at 1513, 1422, and 1347 cm^{-1} corresponding to monodentate carbonates were observed at 423 K. The intensity of these three bands increased significantly upon heating, and by 573 K they were the dominant species on the surface.

Adsorbed carbon monoxide was observed at 373 K, with bands at 2039 (linear) and 1897 (bridged) cm^{-1}. Increasing the temperature to 423 K resulted in the disappearance of the band at 1897 cm^{-1} while the band at 2039 cm^{-1} developed into two bands, at 2097 and 2018 cm^{-1}. These two new bands intensified upon heating to 473 K but were weaker at 523 K, with a concomitant shift to 2066 and 2016 cm^{-1}. The simultaneous behavior of the bands at 2097 and 2018 cm^{-1} may indicate the presence of *gem*-dicarbonyl species; however the lower frequency band is situated lower than expected for an asymmetric dicarbonyl stretch (ca. 10 cm^{-1}). The intensities of both the asymmetric and symmetric stretches of true *gem*-dicarbonyl species are equal, and according to the spectrum shown in Fig. 3 (423 K) the band at 2018 cm^{-1} is much stronger than that at 2097 cm^{-1}, which may indicate an overlap of several bands.

There is precedence in the literature for the observation of *gem*-dicarbonyl bands at low frequency. Dai and Worley (28), studying acetaldehyde decomposition over 2.2% Rh/Al_2O_3, observed twin adsorbed CO bands, at 2082 and 2012 cm^{-1}. Generally, twin bands that appear at 2100 and 2030 cm^{-1} are indicative of the presence of rhodium (+1) *gem*-dicarbonyl species. Both of the dicarbonyl bands observed by Dai and Worley appeared 18 cm^{-1} lower and the

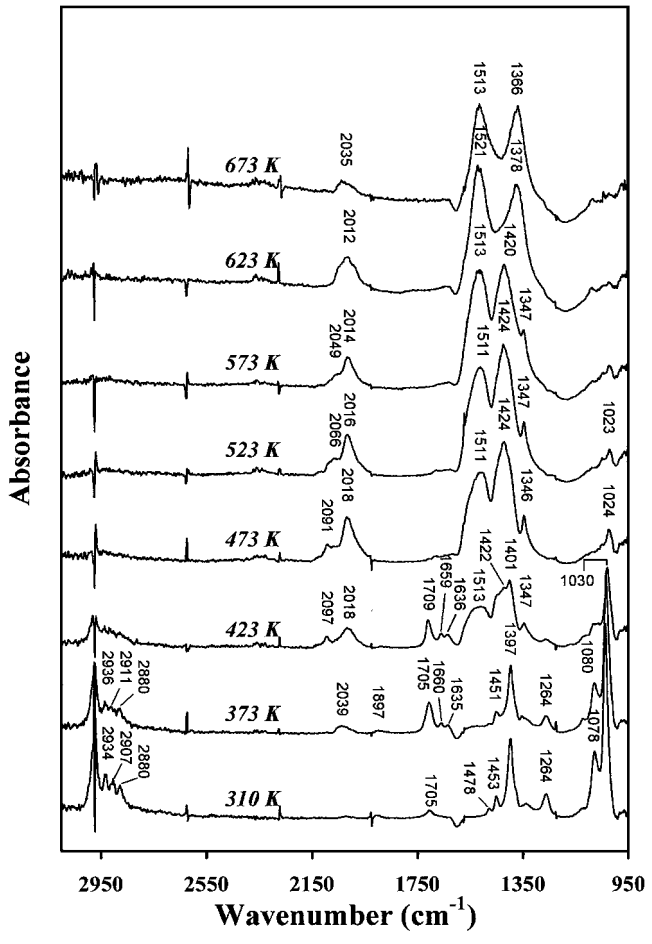

FIG. 3. FTIR after ethanol adsorption at 310 K over unreduced Rh–Pt/CeO_2.

authors postulated that acetaldehyde decomposition over Rh/Al_2O_3 yielded a rhodium *gem*-dicarbonyl species with Rh in a zero oxidation state. Yates and Cavanagh (29) have also observed abnormally low frequency bands (2088 and 2021 cm^{-1}) for Rh dicarbonyl species during the decomposition of formaldehyde over 2.2% Rh/Al_2O_3. The low frequency of these bands was attributed to support perturbations of the CO modes incurred by the presence of oxide-bound species derived from H_2CO. This explanation was supported by studies involving the adsorption of formaldehyde on Rh/Al_2O_3 preadsorbed with CO, which caused a shift to lower wavenumbers of the Rh *gem*-dicarbonyl species.

In this case it is highly unlikely that Rh^0 would be present on the unreduced catalyst, and XPS data (Table 1) show the existence of Rh $3d_{5/2}$ close to 310.0 eV, which is due to RhO_2 (30), while the XPS of Rh^0 $3d_{5/2}$ would be expected at 307 eV. Since considerable amounts of acetaldehyde are formed, it is most likely that perturbation of the CO due to adjacent adsorbed acetaldehyde will result in the downshifting of the bands, as indicated in Ref. (29). Thus, the most likely explanation is the following: two equally intense bands corresponding to Rh^+ *gem*-dicarbonyl species occur, but the one at low wavenumber is masked by a linear CO mode at ca. 2020 cm^{-1}.

At 573 K, the band at 2014 cm^{-1} with a shoulder at 2049 cm^{-1} predominates. This band increased slightly in intensity upon heating to 573 K and was downshifted to 2012 cm^{-1}. By 673 K the band at 2012 cm^{-1} had diminished, with an accompanying shift in frequency to 2035 cm^{-1}.

III.B.iii. Adsorption of ethanol on H_2-reduced Rh–Pt/CeO_2. Figure 4A presents the spectrum obtained after the adsorption of ethanol on H_2-reduced Rh–Pt/CeO_2 at 310 K. Several differences were observed between the adsorption on H_2-reduced Rh–Pt/CeO_2 and that on the unreduced Rh–Pt/CeO_2 surface. In addition to bands corresponding to adsorbed ethoxide species at 1451, 1397, 1075, and 1038 cm^{-1}, a band at 2032 cm^{-1} corresponding to linearly adsorbed CO was also detected. The bands occurring in the spectral range beyond 2700 cm^{-1} are omitted due to the appearance of excessive noise. The temperature variation of the intensities of the IR bands due to ethoxide, adsorbed CO, and carbonate is shown in Fig. 5. Heating the ethanol-treated surface caused a decrease in the intensity of the ethoxide bands, with their complete disappearance at 623 K. At 373 K, the linearly adsorbed CO band increased in intensity and shifted from 2032 cm^{-1} to 2037 cm^{-1} (Fig. 4). Evidence of more than one mode of linearly adsorbed CO can be seen by the presence of a shoulder (at 1990 cm^{-1}) at 473 K and above. The intensity of the band peaked at 523 K with a shift to a lower wavenumber of 2015 cm^{-1}, and by 673 K the band had diminished considerably. Carbonates were the predominant decomposition product at higher temperatures. Monodentate carbonate species were detected at 473 K by bands at 1520, 1424, and 1349 cm^{-1}; these bands intensified significantly with increasing temperature and by 573 K (Fig. 4B) two strong bands, at 1520 and 1418 cm^{-1} (with a shoulder at 1370 cm^{-1}), were observed. At 673 K the band at ca. 1420 cm^{-1} decreased considerably in intensity while the shoulder had developed into an intense band. By 673 K only the bands at 1515 and 1370 cm^{-1} were observed.

Unlike the unreduced surface, no evidence of acetaldehyde or crotonaldehyde formation was observed. However, a broad band at 1694 cm^{-1} was detected at 373 K, and with further increase in temperature this shifted to 1707 cm^{-1} and developed a shoulder at 1752 cm^{-1} (Fig. 4A). The intensity of the bands at 1707 and 1752 cm^{-1} increased upon heating to 523 K (Fig. 4B) and the band at 1707 cm^{-1} was downshifted to 1680 cm^{-1}. The bands at 1680 and 1752 cm^{-1} decreased in intensity upon further heating and disappeared by 623 K.

Similar bands have been observed upon adsorption of CO on H_2-reduced Pt–Na/CeO_2 (1776 and 1690 cm^{-1}), Pt–Na/SiO_2 (1790 cm^{-1}), and Pt/CeO_2 (1690 cm^{-1}) (31).

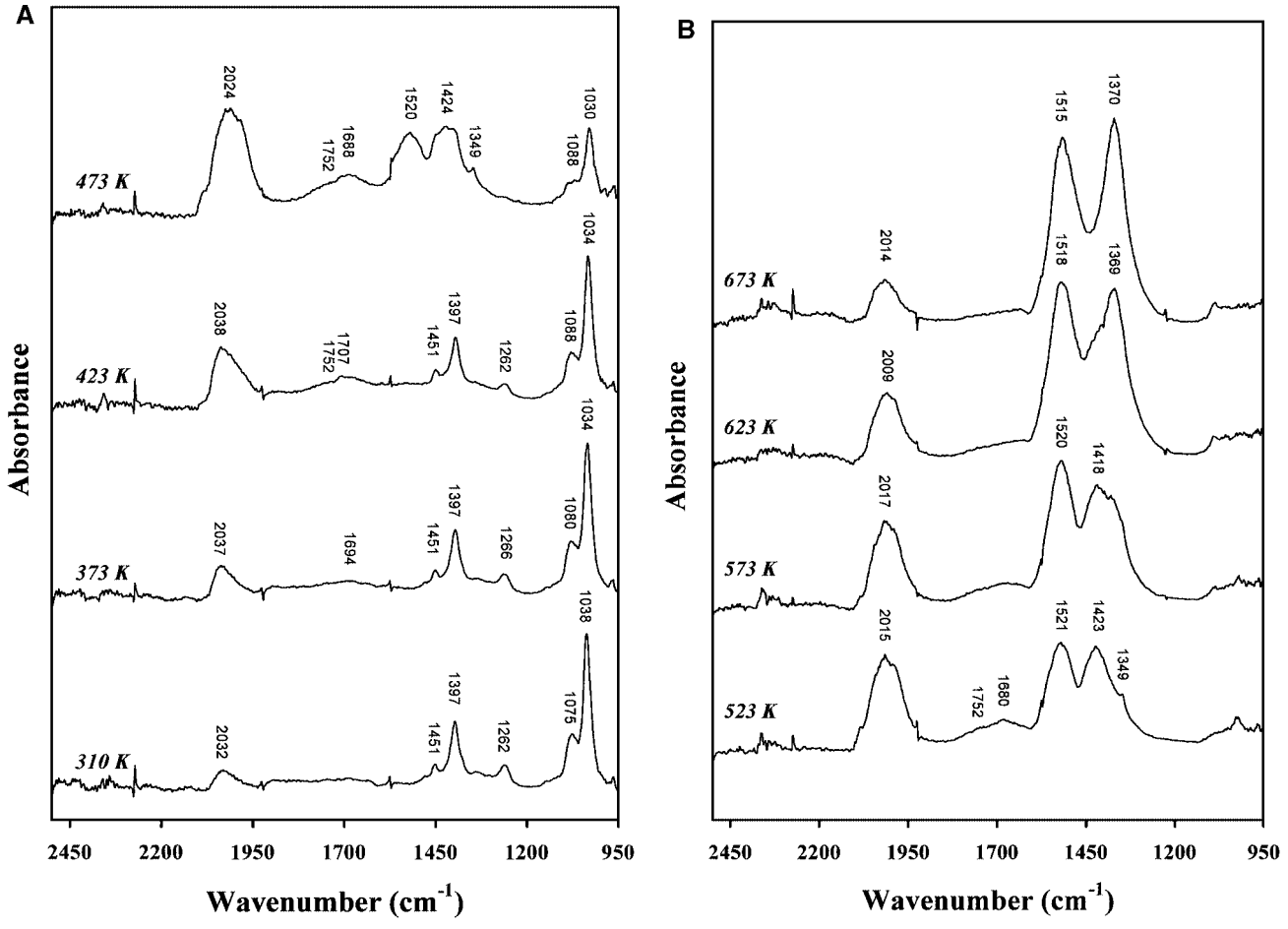

FIG. 4. (A) FTIR after ethanol adsorption at 310 K over H_2-reduced Rh–Pt/CeO_2 and subsequently annealed to the indicated temperature (310–473 K). (B) FTIR after ethanol adsorption at 310 K over H_2-reduced Rh–Pt/CeO_2 and subsequently annealed to the indicated temperature (523–673 K).

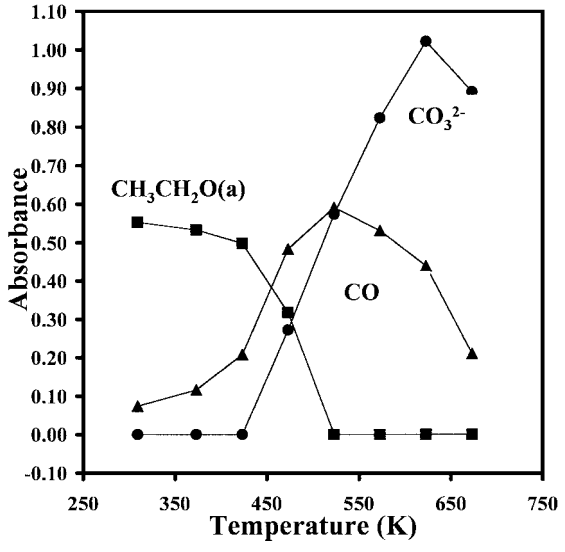

FIG. 5. Plot of the intensities of bands attributed to ethoxides, CO, and CO_3^{2-} species, formed from ethanol over H_2-reduced Rh–Pt/CeO_2, as a function of temperature.

Lavalley *et al.* (32) have also reported bands at 1725 and 1696 cm^{-1} upon adsorption of CO on Rh–Ce/SiO_2 and Rh/CeO_2, respectively. These bands have been attributed to a CO species bonded through both the carbon and oxygen atoms to the surface in such a way that the metal atoms and the surface atoms of the support are both involved, as represented in Scheme 1. Such bands were not observed in previous studies of ethanol adsorption on the surfaces of

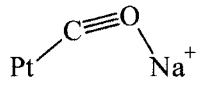

1790 cm^{-1} (Pt-Na/SiO_2)
1776 cm^{-1} (Pt-Na/CeO_2)

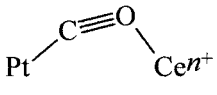

1690 cm^{-1} (Pt/CeO_2)
1690 cm^{-1} (Pt-Na/CeO_2)

SCHEME 1. Tilted CO species observed upon adsorption of CO on the surfaces of Pt/CeO_2 and promoted Pt–Na/SiO_2 and Pt–Na/CeO_2 (31, 32).

unreduced CeO_2 (8), Pd/CeO_2 (8), Pt/CeO_2 (22), Rh/CeO_2 (23), or Pd–Rh/CeO_2 (25). However, adsorption of CO on H_2-reduced Pt/CeO_2 (22) and Rh/CeO_2 (33) did yield similar bands at 1790–1700 cm^{-1} corresponding to C- and O-adsorbed CO species.

Hence, the bands observed at 1752 and 1680 cm^{-1} are attributed to tilted CO species adsorbed to the surface through both the C and O ends of the molecule. What the exact site of adsorption is, be-it Rh–CO–Ce^{n+}, Rh_2–CO–Ce^{n+}, Pt–CO–Ce^{n+}, Pt_2–CO–Ce^{n+}, Rh–CO–Rh, Rh–CO–Pt, or Pt–CO–Pt, is beyond the scope of this work.

III.C. Steady-State Reactions: Ethanol Reaction over Rh–Pt/CeO_2 (Ethanol : O_2 = 1 : 2, Molar Ratio)

Figure 6 shows a plot of the product concentrations as a function of temperature at a feed stream of 1 : 2 ethanol-to-molecular oxygen ratio over Rh–Pt/CeO_2. The main objective was to follow any reaction products formed from ethanol reactions. Methane was detected in trace amounts at 473 K and in substantially increasing amounts by 573 K, while a considerable decrease occurred in the amounts of both ethanol and acetaldehyde. At 673 K, traces of acetone, together with small amounts of acetaldehyde, were detected, while the amount of methane slightly increased. The concomitant formation of acetone and acetaldehyde may indicate a common intermediate. The formation of acetone at 673 K is very similar to that previously observed for acetaldehyde-TPD on CeO_2 (7), suggesting that this channel occurs on the support. Acetaldehyde is thus most likely formed by oxidative dehydrogenation of ethanol on CeO_2. Part of this is oxidized to acetates, which combine together to yield acetone and CO_2 (ketonization reaction). At 773 K, all four products decreased in concentration and this trend continued with further heating to 873 K. At 873 K, acetone was no longer detected, and by 973 K, methane was the only detected hydrocarbon.

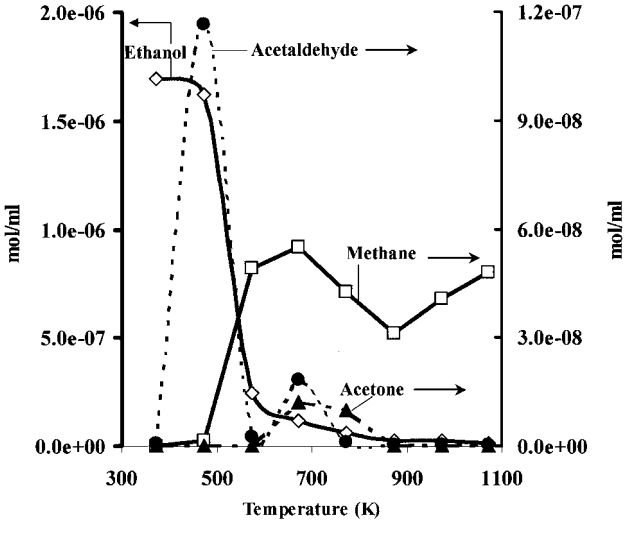

FIG. 6. A plot of the products concentration as a function of temperature at a feed stream of a 1 : 2 ethanol-to-molecular oxygen ratio over Rh–Pt/CeO_2.

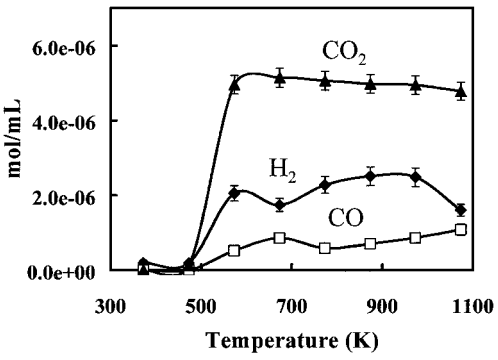

FIG. 7. A plot of the formation of H_2, CO, and CO_2 from a 1 : 2 ethanol-to-molecular oxygen feed stream ratio over Rh–Pt/CeO_2 as a function of temperature.

Figure 7 shows a plot of the formation of H_2, CO, and CO_2 from a 1 : 2 ethanol-to-molecular oxygen feed stream ratio over Rh–Pt/CeO_2 as a function of temperature. Only traces of hydrogen, carbon dioxide, and carbon monoxide were observed up to 473 K. At 573 K, a sharp increase in carbon dioxide concentration and a gradual increase in hydrogen concentration were observed. At 673 K, the hydrogen concentration showed a small decrease. Carbon dioxide slowly decreased with further heating to 1073 K (while the effect of increased temperature on CO was in the opposite direction). The hydrogen concentration began to increase again at 773 K and steadily increased up to 973 K. Molar yields are given in Table 5.

Although the stoichiometric ratio of 3/2 O_2 to 1 ethanol is theoretically best for hydrogen production we have observed a better catalytic stability (within the experimental time—a few hours) using a ratio of 2. Some experiments were conducted to check for carbon deposition. After 265 min of reaction, the ethanol was stopped and only O_2 was allowed into the reactor, to oxidize any carbon deposited to CO_2. The total amount of CO_2 formed was found negligible. An estimation of water formation was done by mass balance. For example, at 973 K the total mass of products was found to be equal to 0.25 g/L, given by subtraction from the inlet (0.36 g/L) 0.11 g/L of water.

IV. DISCUSSION

The main result of this work is that efficient decomposition of ethanol, together with hydrogen production, requires the presence of both Rh and Pt. This is manifested by a decrease of the activation energy of the reaction (Table 1) and the absence of (or considerable decrease in) the amount of secondary products resulting from acetaldehyde (such as benzene, ketene, and crotonaldehyde).

TABLE 5

Mole Percent Yield of Products from Ethanol Reaction over Rh–Pt/CeO_2

Product	473 K	573 K	673 K	773 K	873 K	973 K	(973 K)[a]	1073 K
CH_3CHO	45.9	0.06	0.45	0.02	0.01	0.01	Traces	0.01
	48.7[b]	0.9[b]	2.72[b]	0.7[b]	—	—		—
CH_4	5.1	10.7	11.1	9.0	6.6	8.3	0.0109	10.4
	10.8[b]	17.7[b]	17.1[b]	15.8[b]	12.0[b]	9.1[b]	0.0094[b]	9.5[b]
$CH_3C(O)CH_3$	—	—	0.4	0.4	—	—	—	
			1.2[b]	2.3[b]				
CO	—	6.8	10.5	7.4	9.0	10.6	0.024	14.0
		15.3[b]	13.3[b]	12.1[b]	12.1[b]	13.1[b]	0.024[b]	16.3[b]
CO_2	23.8	64.6	63.1	64.0	63.2	60.7	0.218	61.8
	32.6[b]	61.7[b]	58.3[b]	57.5[b]	58.8[b]	60.3[b]	0.172[b]	59.9[b]
H_2	25.2	17.9	14.3	19.2	21.2	20.3	0.005	13.8
	7.8[b]	4.4[b]	7.4[b]	11.7[b]	17.1[b]	17.6[b]	0.003[b]	14.4[b]
Conversion, %	10.5	92.7	96.8	98.2	99.2	99.2		99.6
	12.9[b]	88.4[b]	92.4[b]	97.5[b]	98.6[b]	98.6[b]		98.5[b]
K_p[c]	210.8	38.83	11.72	4.90	2.55	1.54		1.04

[a] Mass of products in grams per liter.
[b] With O_2-to-EtOH ratio = 1.5.
[c] Equilibrium constant for the CO conversion reaction (shift), from Ref. (39). $CO + H_2O \rightleftharpoons CO_2 + H_2$. $K_p = p_{H_2} p_{CO_2} / p_{H_2O} p_{CO}$.

The other key observations of this work are as follows.

1. While adsorbed acetaldehyde was the main species formed on nonreduced catalysts, adsorbed CO was the main species formed on the reduced ones.

2. Hydrogen desorbs in three temperature domains during TPD. The first two are the same as those of acetaldehyde. This hydrogen desorption is attributed to ethanol dehydrogenation on Pt and Rh particles. The third desorption of hydrogen (at 650 K) appears alone and is most likely associated with some trace amounts of ethanol on the surface of CeO_2 that has been dehydrogenated. The desorption of water in the same temperature domain indicates that large amounts of H_2 have been oxidized to water during TPD.

3. Ethylene was not observed in any of the TPD or steady state catalytic reactions. This is consistent with previous work on CeO_2 and M/CeO_2 (8, 22, 23). Unlike Al_2O_3 (acidic support favoring dehydration reactions (3, 6)) CeO_2 mainly favours dehydrogenation reactions. This is in fact important since any olefin formed may further react to make polymers that eventually block the reactor.

4. Tilted CO was observed on hydrogen-reduced Rh–Pt/CeO_2.

Why Rh–Pt is efficient for carbon–carbon bond dissociation reactions is a key question. In order to decompose the carbon–carbon bond of an ethoxy species, orbital–orbital interaction between the carbon atoms of the adsorbate and the surface is required. This may only happen if the adsorbed species is tilted toward the surface. Study of the reaction pathway of ethanol over a Rh(111) single crystal, a flat surface, has shown that this is indeed the case (34–36). While on Pt or Pd adsorbed ethanol is dissociated to give ethoxides that further react with the surface to give acetaldehyde, Rh has shown a different pathway. Ethoxide species lose one hydrogen from the terminal (methyl) group and are thus adsorbed in a cyclic configuration onto the surface (oxametallacycle intermediate) (34–36). (Rh metal is known to activate the carbon–hydrogen sp^3 bonds (37, 38)). Oxametallacycle formation has been well documented experimentally by HREELS on Rh(111) single-crystal surfaces and later by DFT calculation of clusters (34–36). It has been demonstrated that the five-membered-ring oxametallacycle intermediate is more stable on Rh (as well as on Ni) than η^1 (or η^2)-adsorbed acetaldehyde (see Scheme 2).

Because of the IR setup in this work (windows cut off at 1000 cm^{-1}) the stretching and bending modes of the oxametallacycle that occur below 1000 cm^{-1} could not be detected; the frequency of the modes expected for the five-membered-ring oxametallacycle species above 1000 cm^{-1} (35) are similar to those for ethoxides.

The proximity of the adsorbed species to the surface may likely contribute to the efficient carbon–carbon bond dissociation. Another requirement is needed to continue the reaction and this is related to the hydrogenation reaction—otherwise surface carbon will build up. In the first step of the (low temperature) dehydrogenation reaction of ethanol to the oxametallacycle and/or acetaldehyde,

$$CH_3CH_2OH \rightarrow CH_3CH_2O(a) + H(a), \quad [5]$$

$$CH_3CH_2O(a) \rightarrow (a)CH_2CH_2O(a)/CH_3CHO + H(a), \quad [6]$$

$$2H(a) \rightarrow H_2, \quad [7]$$

where (a) stands for adsorbed. The association reaction of

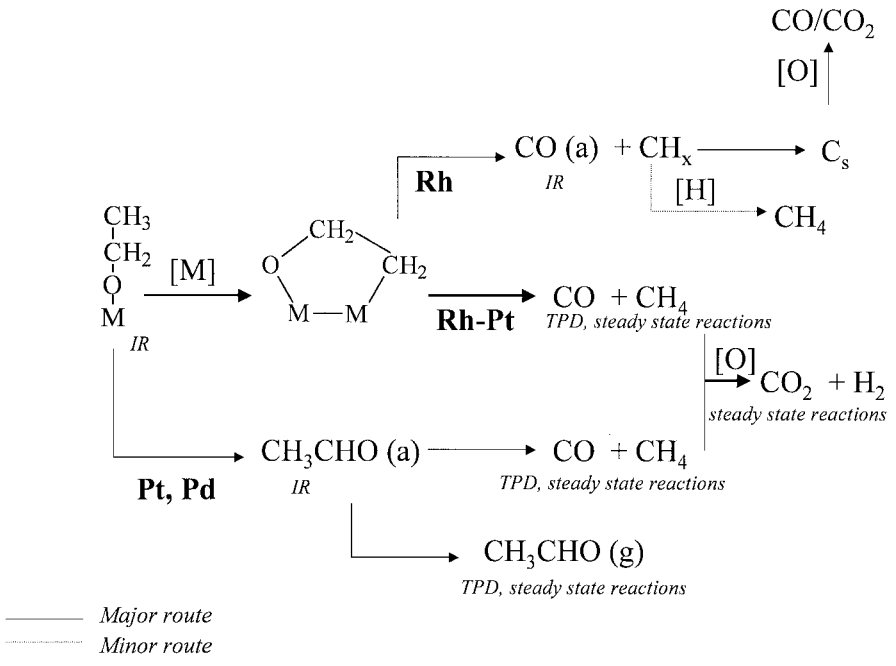

SCHEME 2

the two H(a) atoms is much faster in the presence of Pt. At high temperatures (800 K and above) methane is the only observed hydrocarbon product. The decrease in methane production between 700 and 900 K together with the increase of hydrogen in this temperature domain may indicate that some of the latter has resulted from a partial oxidation of methane (to CO/CO_2). Reforming of methane may as well occur; however water production could not be qualitatively measured in steady state reactions, and on the basis of the present work one cannot understand the effect of water on H_2 production on these Rh–Pt/CeO_2 materials. The amount of CO_2 formed was found to be very sensitive to the gas-phase concentration of O_2 at low temperatures (up to ca. 773 K).

A summary of the reaction pathway of ethanol on Rh–Pt/CeO_2 and other monometallic catalysts is given in Scheme 2. On all catalysts investigated so far, ethoxides are the main observed species upon ethanol adsorption at room temperature (8, 22, 23, 33, this work). Adsorbed acetaldehyde is mainly observed on unreduced surfaces. The presence of Rh metal results in considerable formation of CO at low temperatures (310 K) and this can be explained by the decomposition of an intermediate species (such as the five-membered-ring oxametallacycle intermediate). In the absence of a second metal, formation of small amounts of methane is observed. While Rh is essential for an efficient decomposition of ethanol its presence alone is not sufficient for making hydrogen in reasonable quantities. The presence of a second metal (in addition to Rh) such as Pt enhances the production of hydrogen from ethanol.

REFERENCES

1. Freni, S., *J. Power Sources* **94**, 14 (2001).
2. Thomas, J. M., and Thomas, W. J., "Principles and Practice of Heterogeneous Catalysis." VCH, Weinheim/New York, 1997.
3. Velu, S., Suzuki, K., Kapoor, M. P., Ohashi, F., and Osaki, T., *Appl. Catal. A* **213**, 47 (2001).
4. Idriss, H., and Barteau, M. A., *Adv. Catal.* **45**, 261 (2000).
5. Idriss, H., and Seebauer, E. G., *J. Mol. Catal. A* **152**, 201 (2000).
6. Cavallaro, S., *Energy Fuels* **14**, 1195 (2000).
7. Idriss, H., Diagne, C., Hindermann, J. P., Kiennemann, A., and Barteau, M. A., *J. Catal.* **155**, 219 (1995).
8. Yee, A., Morrison, S., and Idriss, H., *J. Catal.* **186**, 279 (1999).
9. Sugiyama, S., Sato, K., Yamasaki, S., Kawashiro, K., and Hayashi, H., *Catal. Lett.* **14**, 127 (1992).
10. Pestman, R., Koster, R. M., van Duijine, A., Pieterse, J. A. Z., and Ponec, V., *J. Catal.* **168**, 265 (1997) and references therein.
11. Idriss, H., and Barteau, M. A., *Catal. Lett.* **40**, 147 (1996).
12. Idriss, H., Kim, K. S., and Barteau, M. A., *J. Catal.* **139**, 119 (1993).
13. Tanabe, K., and Saito, K., *J. Catal.* **35**, 247 (1974).
14. Idriss, H., and Seebauer, E. G., *Catal. Lett.* **66**, 139 (2000).
15. Peng, X. D., and Barteau, M. A., *Langmuir* **5**, 1051 (1989).
16. Lavalley, J. C., Lamotte, J., Busca, G., and Lorenzelli, V., *J. Chem. Soc. Chem. Commun.* 1006 (1985).
17. Idriss, H., Pierce, K., and Barteau, M. A., *J. Am. Chem. Soc.* **116**, 3063 (1994).
18. Cong, Y., and Masel, R. I., *Surf. Sci.* **396**, 1 (1998).
19. Sexton, B. A., Rendulic, K. D., and Hughes, A. Z., *Surf. Sci.* **181**, 1212 (1982).
20. Davis, J. L., and Barteau, M. A., *Surf. Sci.* **187**, 388 (1987).
21. Gates, S. M., Russell, J. N., Jr., and Yates, J. T., Jr., *Surf. Sci.* **171**, 111 (1986).
22. Yee, A., Morrison, S., and Idriss, H., *J. Catal.* **191**, 30 (2000).
23. Yee, A., Morrison, S., and Idriss, H., *Catal. Today* **63**, 327 (2000).
24. Luo, H. Y., Zhang, W., Zhou, H. W., Huang, S. Y., Lin, P. Z., Ding, Y. J., and Lin, L. W., *Appl. Catal. A* **214**, 161 (2001).

25. Yee, A., Morrison, S., and Idriss, H., *in* "16th North American Catalysis Society Meeting, Boston, MA, May–June, 1999," poster presentation number PI-067.
26. Ko, E. I., Benziger, J. B., and Madix, R. J., *J. Catal.* **62**, 264 (1980).
27. Greenler, N. P. G., "Guide to the Complete Interpretation of Infrared Spectra of Organic Structures." Wiley, New York, 1994.
28. Dai, C. H., and Worley, S. D., *Langmuir* **4**, 326 (1988).
29. Yates, J. T., and Cavanagh, R. R., *J. Catal.* **74**, 97 (1982).
30. Briggs, D., and Seah, M. P., "Practical Surface Analysis," 2nd ed. Wiley, Chichester, 1996.
31. Boujana, S., Demri, D., Cressely, J., Kiennemann, A., and Hindermann, J. P., *Catal. Lett.* **7**, 359 (1990).
32. Lavalley, J. C., Saussey, J., Lamotte, J., Breault, R., Hindermann, J. P., and Kiennemann, A., *J. Phys. Chem.* **94**, 5941 (1990).
33. Yee, A., M.Sc. dissertation. University of Auckland, 1999 and in preparation.
34. Brown, N. F., and Barteau, M. A., *Langmuir* **11**, 1184 (1995).
35. Jones, G. S., Mavrikakis, M., Barteau, M. A., and Vohs, J. M., *J. Am. Chem. Soc.* **120**, 3196 (1998).
36. Mavrikakis, M., Doren, D. J., and Barteau, M. A., *J. Phys. Chem.* **102**, 394 (1998).
37. Atherton, M. J., Fawcett, J., Holloway, J. H., Hope, E. G., Martin, S. M., Russell, D. R., and Suanders, G. C., *J. Organomet. Chem.* **555**, 67 (1998).
38. Atherton, M. J., Fawcett, J., Holloway, J. H., Hope, E. G., Karacar, A., Russell, D. R., and Suanders, G. C., *J. Chem. Soc. Dalton Trans.* **15**, 3215 (1996).
39. Twigg, M. V., Ed., "Catalyst Handbook," 2nd ed. Wolfe, Frome, England, 1989.